Adsorption Properties of Keggin-type Polyoxometalates on Carbon Based Electrode Surfaces and Their Electrocatalytic Activities

Suhee Choi and Jongwon Kim*

Department of Chemistry, Chungbuk National University, Cheongju, Chungbuk 361-763, Korea
**E-mail: jongwonkim@chungbuk.ac.kr*
Received December 15, 2008, Accepted February 19, 2009

The interactions between four Keggin-type POMs ($SiW_{12}O_{40}^{4-}$, $PW_{12}O_{40}^{3-}$, $SiMo_{12}O_{40}^{4-}$, and $PMo_{12}O_{40}^{3-}$) and glassy carbon (GC) and highly oriented pyrolytic graphite (HOPG) surfaces are investigated in a systematic way. Electrochemical results show that molibdate series POMs adsorb relatively stronger than tungstate POMs on GC and HOPG surfaces. Adsorption of POMs on HOPG electrode surfaces is relatively stronger than on GC surfaces. $SiMo_{12}O_{40}^{4-}$ species exhibits unique adsorption behaviors on HOPG surfaces. Surface-confined $SiMo_{12}O_{40}^{4-}$ species on HOPG surfaces exhibit unique adsorption behaviors and inhibit the electron transfer from the solution phase species. The catalytic activity of the surface-confined POMs for hydrogen peroxide electroreduction is also examined, where $PW_{12}O_{40}^{3-}$ species adsorbed on GC surfaces exhibits the highest catalytic efficiency among the investigated POM modified electrode systems.

Key Words: Polyoxometalate, Glassy carbon, Highly oriented pyrolytic graphite, Adsorption, Electrocatalysis

Introduction

Polyoxometalates (POMs), constituting a large class of metal oxide molecules, have a variety of structures, sizes, chemical reactivities, and electrochemical properties.[1] Since POMs have many practical applications such as heterogeneous catalysis[2] and molecular materials,[3] the modification of electrode surfaces with POMs have been widely investigated. It has been known that POM anions spontaneously adsorb on various electrode surfaces such as Au, Ag, and carbon. Among the various kinds of POMs for electrode surface modifications, Keggin-type POMs were the most widely investigated. Figure 1 shows the structure of a Keggin-type POM, which consists of a centered metal atom, addenda metal atoms, and oxygens. Depending on the composition of centered and addenda metal species, various Keggin-type POMs have been synthesized and characterized, however, four representative POMs were widely utilized for electrode modifications. The first two POMs are tungstate series, silicotungstate ($SiW_{12}O_{40}^{4-}$) and phospotungstate ($PW_{12}O_{40}^{3-}$), while the other two POMs are molibdate series, silicomolibdate ($SiMo_{12}O_{40}^{4-}$) and phospomolibdate ($PMo_{12}O_{40}^{3-}$).

Keita and Nadjo pioneered the electrochemical applications of Keggin-type POMs. They reported based on electrochemical quartz crystal microbalance (EQCM) results that $SiW_{12}O_{40}^{4-}$ adsorbs spontaneously on Au surfaces, while its reduced species desorbs from the Au surfaces.[4] Anson and co-workers showed that $PMo_{12}O_{40}^{3-}$ strongly adsorbs on glassy carbon and pyrolytic graphite electrode surfaces.[5] The $PMo_{12}O_{40}^{3-}$-modified carbon electrode surface exhibits electrocatalytic activity for hydrogen peroxide reduction.[6] The monolayer structures of POMs on electrode surfaces were intensively investigated by Gewirth and co-workers. For example, they reported the scanning tunneling microscopy (STM) images of well ordered monolayers of $SiW_{12}O_{40}^{4-}$ adsorbs on Ag and Au surfaces.[7,8] It was reported that the interaction between $SiW_{12}O_{40}^{4-}$ and Ag surfaces is quite unique that the adsorbed $SiW_{12}O_{40}^{4-}$ species passivate the Ag electrode toward subsequent solution redox chemistry.[9]

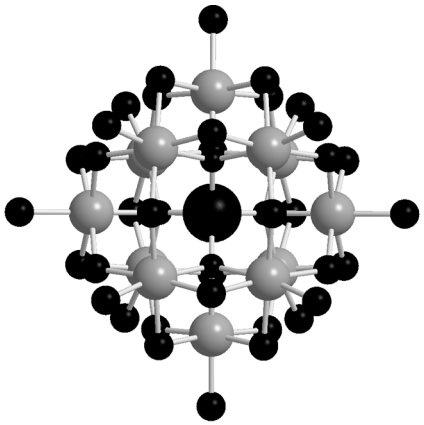

Figure 1. Structure of a Keggin-type polyoxometalate. Large black, small black, and gray circles correspond to centered metal, oxygen, and addenda metal atoms, respectively.

The ability of POMs to adsorb on electrode surfaces has been applied to fabricating composite POM-nanomaterials based on carbon nanotubes and Au nanoparticles. Phospomolibdate POM, $PMo_{12}O_{40}^{3-}$, was utilized to prepare two-dimensional graphite sheets by exfoliation of highly oriented pyrolytic graphite (HOPG).[10] Carbon nonotubes have been modified with Keggin-type POMs such as $PMo_{12}O_{40}^{3-}$ and $SiW_{12}O_{40}^{4-}$, which exhibited electrocatalytic activities.[11,12] It was also shown that Au nanoparticles can be modified with a layer of $PMo_{12}O_{40}^{3-}$ and utilized for electrocatalytic reduction of bromate ions.[13] Keggin-type POM-modified Pt nanoparticles were demonstrated to produce highly reactive platinum centers toward electroreduction of oxygen.[14] Although there

have been several applications based on interactions between Keggin-type POMs and electrode surfaces, most of them focused on $PMo_{12}O_{40}^{3-}$ species. In this report, we performed a systematic study on general adsorption behaviors of four Keggin-type POMs on GC and HOPG electrode surfaces. The interaction behaviors between POMs and carbon based electrodes, especially HOPG surfaces would be important considering that carbon based nanomaterials such as carbon nanotubes and graphenes are widely utilized for fabricating functional materials. The absorption behaviors of different Keggin-type POMs are characterized by electrochemical methods and compared with each other. The electrocatalytical activities of adsorbed POM species toward electroreduction of hydrogen peroxide are investigated.

Experimental

All solutions were prepared using purified water (Milli-Q, 18.2 MΩ·cm). The supporting electrolyte was 0.1 M H_2SO_4 (Merck). POM solutions were prepared from $H_4SiW_{12}O_{40}$, $H_3PW_{12}O_{40}$, $H_4SiMo_{12}O_{40}$, and $H_3PMo_{12}O_{40}$ (Aldrich) and the typical concentration was 1 mM. A commercially available glassy carbon (GC) electrode (CH Instrument, 3 mm in diameter) was employed. The surface was mechanically polished with alumina powder from a lager particle size down to a smallest one (*ca*. 0.3 μm) on a Microcloth pad (Buehler). Between each polishing step the electrode was sonicated for 5 min in Milli-Q water. HOPG was obtained from TAAB Laboratories Equipment Ltd. (Berkshire, UK), and clean surfaces were prepared by cleaving a fresh surface using Scotch tape to give a flat, shiny surface immediately before use. The fresh HOPG surface was confined in an O-ring with an inner diameter of 2.9 mm and used as a working electrode. Electrochemical measurements were conducted using a BAS 100BW potentiostat (Bioanalytical Systems, West Lafayette, IN) and the solution was purged with N_2 prior to use. Pt wire and Ag/AgCl electrodes were used as counter and reference electrodes, respectively. All potentials are reported relative to the Ag/AgCl reference electrode (3 M KCl). For calibration plots, the working electrode was rotated using a Pine model MSRX rotator.

Results and Discussion

Adsorption behavior of Keggin POMs on GC electrode surfaces. Figure 2 shows the electrochemical responses of four different Keggin-type POMs on GC electrode surfaces. Solid lines were obtained from solutions containing a 1 mM POM + 0.1 M H_2SO_4. For tungstate series POMs ($SiW_{12}O_{40}^{4-}$ and $PW_{12}O_{40}^{3-}$), three well-defined redox waves were observed as shown in Figure 2A and B, which correspond to one-, one-, and two-electron processes, respectively.[15] Molibdate series POMs ($SiMo_{12}O_{40}^{4-}$ and $PMo_{12}O_{40}^{3-}$) exhibit redox waves at more positive potential regions than those found from tungstate POMs. All of the three redox waves obtained from $SiMo_{12}O_{40}^{4-}$ are known to be two-electron processes.[15] In the case of $PMo_{12}O_{40}^{3-}$, the solution-phase cyclic voltammogram is not well-defined as shown in Figure 2D due to the easy hydrolysis of $PMo_{12}O_{40}^{3-}$ in aqueous electrolytes. Midpoint potentials (E_{mid}) and peak separations (ΔE_p) for solution-phase cyclic voltammograms of POMs on GC electrodes are tabulated in Table 1. Here, $E_{mid} = (E_c + E_a)/2$, where E_c and E_a are the cathodic and anodic peak potentials, respectively.

Table 1. Midpoint potentials (E_{mid}) and peak separations (ΔE_p) for solution-phase cyclic voltammograms of POMs on GC and HOPG electrodes

Electrode	POM	First wave		Second wave		Third wave	
		E_{mid}[a] (V)	ΔE_p[b] (mV)	E_{mid}[a] (V)	ΔE_p[b] (mV)	E_{mid}[a] (V)	ΔE_p[b] (mV)
GC	$SiW_{12}O_{40}^{4-}$	-0.175	65	-0.415	70	-0.595	40
	$PW_{12}O_{40}^{3-}$	0.036	67	-0.244	67	-0.618	45
	$SiMo_{12}O_{40}^{4-}$	0.327	38	0.212	48	0.038	43
	$PMo_{12}O_{40}^{3-}$	[d]		0.184	51	[d]	
HOPG	$SiW_{12}O_{40}^{4-}$	-0.229	123	-0.461	96	-0.636	70
	$PW_{12}O_{40}^{3-}$	-0.021	105	-0.287	93	-0.650	58
	$SiMo_{12}O_{40}^{4-}$	0.289	69	0.185	83	[d]	
	$PMo_{12}O_{40}^{3-}$	[d]		0.174	111	[d]	
ΔEmid[c] (mV)	$SiW_{12}O_{40}^{4-}$	54		46		41	
	$PW_{12}O_{40}^{3-}$	56		44		33	
	$SiMo_{12}O_{40}^{4-}$	38		27		38	
	$PMo_{12}O_{40}^{3-}$			11			

[a] $E_{mid} = (E_c + E_a)/2$, where E_c and E_a are the cathodic and anodic peak potentials, respectively. [b] $\Delta E_p = E_c - E_a$. [c] $\Delta E_{mid} = E_{mid}$(GC) − E_{mid}(HOPG). [d] Not available due to ill-defined redox waves.

The dotted lines in Figure 2 were obtained from a pure electrolyte solution on GC electrodes emersed from POM containing solutions after voltammetric measurements (solid lines) and rinsed with electrolyte solutions. The peak positions of the redox waves shown in dotted lines are close to those found from solution-phase cyclic voltammograms. The insets in Figure 2 show that the cathodic peak currents of dotted cyclic voltammograms have a linear relationship with scan rates. In addition, the peak separations between cathodic and anodic waves of dotted lines are smaller than those of solid lines. For example, the first redox wave of $SiMo_{12}O_{40}^{4-}$ has a peak separation of 23 mV in the dotted line, while solid line has a peak separation of 38 mV. The scan-rate dependence of the peak current as well as the small peak separation value indicates that the redox waves presented by dotted lines correspond to surface-confined POM species.[16] Midpoint potentials and peak separations for cyclic voltammograms of surface-confined POMs on GC electrodes are tabulated in Table 2. For tungstate series POMs ($SiW_{12}O_{40}^{4-}$ and $PW_{12}O_{40}^{3-}$), only the third redox waves are observed, while all of three redox waves are observed for molibdate series POMs ($SiMo_{12}O_{40}^{4-}$ and $PMo_{12}O_{40}^{3-}$). In a previous study, it was shown that $SiW_{12}O_{40}^{4-}$ passivates the Ag surface and that one redox wave was present, corresponding to a surface-confined species with a peak position the same as that of the second redox couple of $SiW_{12}O_{40}^{4-}$ in the solution phase.[9] Therefore, the absence of the first two redox waves of tungstate POMs confined on GC electrode surfaces might be ascribed to the passivation of the electrode surface upon adsorption of POMs. Despite the

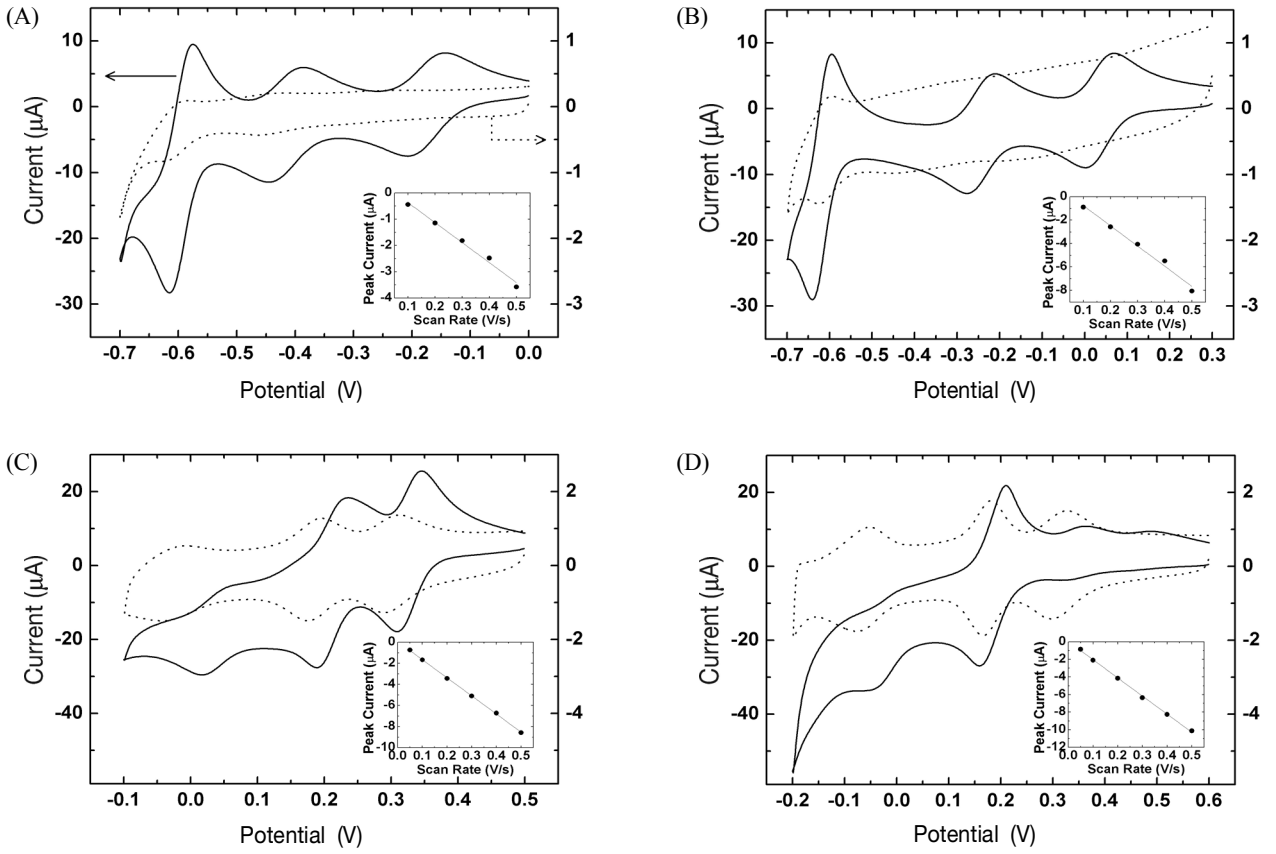

Figure 2. Cyclic voltammograms obtained from (solid line, left current axis) 1 mM POM + 0.1 M H_2SO_4 solutions on GC electrodes and (dotted line, right current axis) 0.1 M H_2SO_4 solutions on POM-adsorbed GC electrodes. (A) $SiW_{12}O_{40}^{4-}$, (B) $PW_{12}O_{40}^{3-}$, (C) $SiMo_{12}O_{40}^{4-}$, and (D) $PMo_{12}O_{40}^{3-}$. The scan rate was 0.05 V/s. The insets show the scan rate dependence of cathodic waves of POM adsorbed on GC electrodes.

Table 2. Midpoint potentials (E_{mid}) and peak separations (ΔE_p) for cyclic voltammograms of surface-confined POMs on GC and HOPG electrodes.

Electrode	POM	First wave		Second wave		Third wave		Relative surface coverage[a]
		E_{mid}[a] (V)	ΔE_p[b] (mV)	E_{mid}[a] (V)	ΔE_p[b] (mV)	E_{mid}[a] (V)	ΔE_p[b] (mV)	
GC	$SiW_{12}O_{40}^{4-}$	[d]		[d]		-0.605	39	0.09
	$PW_{12}O_{40}^{3-}$	[d]		[d]		-0.610	29	0.14
	$SiMo_{12}O_{40}^{4-}$	0.301	23	0.185	21	-0.025	38	0.43
	$PMo_{12}O_{40}^{3-}$	0.312	30	0.173	15	-0.064	23	0.64
HOPG	$SiW_{12}O_{40}^{4-}$	[d]		-0.500	32	-0.648	21	0.28
	$PW_{12}O_{40}^{3-}$	[d]				-0.657	37	0.25
	$SiMo_{12}O_{40}^{4-}$	0.274	12	0.157	11	-0.048	13	0.65
	$PMo_{12}O_{40}^{3-}$	0.309	31	0.167	18	-0.088	27	0.68
ΔE_{mid} (mV)	$SiW_{12}O_{40}^{4-}$					43		
	$PW_{12}O_{40}^{3-}$					47		
	$SiMo_{12}O_{40}^{4-}$	27		29		23		
	$PMo_{12}O_{40}^{3-}$	4		5		23		

[a]$E_{mid} = (E_c + E_a)/2$, where E_c and E_a are the cathodic and anodic peak potentials, respectively. [b]$\Delta E_p = E_c - E_a$. [c]$\Delta E_{mid} = E_{mid}$ (GC) − E_{mid} (HOPG). [d]Not available due to ill-defined redox waves.

solution-phase cyclic voltammogram $PMo_{12}O_{40}^{3-}$ is not well-defined, surface-confined species exhibits three well-defined redox waves as shown in Figure 2D. This phenomenon was also observed on HOPG surfaces (vide infra) and has been also reported by Anson *et al.*[5]

The surface coverage of POMs on electrode surfaces can be evaluated from the charge density under the redox peaks of dotted lines in Figure 2. It has been reported that $SiW_{12}O_{40}^{4-}$ forms a square adlattice on Ag and Au electrode surfaces with inter-molecular spacing of *ca.* 1 nm.[7,17] Assuming that Keggin-type POMs have a similar square type adlattice structure on GC electrode surface, a full monolayer of POMs has a surface density of 1.7×10^{-6} mol/m^2. In the case of $SiMo_{12}O_{40}^{4-}$, the charge density under the first cathodic peak in the dotted line

of Figure 2C is calculated to be 0.14 C/m^2. Considering that this cathodic peak is a two electron process, the surface density of $SiMo_{12}O_{40}^{4-}$ species on a GC electrode is 7.3×10^{-7} mol/m^2. This corresponds around 0.43 monolayer coverage. The relative surface coverage for other POMs are evaluated in the same way and tabulated in Table 2. In multiple measurements, we found that there is *ca* 20% of variation in the surface coverage of POMs adsorbed on GC surfaces from the tabulated values. This inconsistency probably relates to different surface conditions of GC electrodes after mechanical polishing with alumina powders. Despite this inconsistency in the surface coverage, the amount of molibdate POMs adsorbed on GC surfaces is larger than that of tungstate POMs.

It has been reported that tungstate POMs strongly adsorb on Ag surfaces. The interaction between tungstate POMs and Au surface is relatively weaker and no surface-confined species are observed in cyclic voltammograms.[8,9,18] From this study, the interaction between tungstate POMs and GC surfaces seems to be weaker than Ag surfaces, but stronger than Au surfaces. For molibdate POMs, $PMo_{12}O_{40}^{3-}$ species has been widely utilized for surface modifications on Au nanoparticles and carbon nanotubes.[11,13] In this study, we show that $SiMo_{12}O_{40}^{4-}$ as well as $PMo_{12}O_{40}^{3-}$ strongly adsorb on GC surface, thus both of molibdate POMs can be utilized for electrode modifications. The molibdate POMs adsorbed on GC electrode surfaces are stable during the repetitive potential cycles in 0.1 M H_2SO_4. Even after mechanical polishing steps, some of molibdate POMs are still left on the electrode surfaces.

Adsorption behavior of Keggin POMs on HOPG electrode surfaces. Figure 3 shows the electrochemical responses of four different Keggin-type POMs on HOPG electrode surfaces. The solution-phase cyclic voltammograms of POMs on HOPG electrodes (solid lines) show similar electrochemical behaviors compared to those obtained on GC electrode surfaces. Midpoint potentials and peak separations for solution-phase cyclic voltammograms of POMs on HOPG electrodes are tabulated in Table 1. Midpoint potentials of POMs on HOPG electrodes are negatively shifted from those on GC electrodes. The difference in midpoint potentials between GC and HOPG electrodes (ΔE_{mid}) ranged from 11 to 56 mV as shown in Table 1. It is known that heterogeneous electron transfer on a basal plane of HOPG surfaces is slower than that on GC electrode surfaces, which explains the negative potential shifts of redox waves on HOPG compared to those on GC electrodes.[19,20] The slow electron transfer kinetics on HOPG is also corroborated by an increment in peak separation compared to the case of GC electrodes.

The dotted lines in Figure 3 were obtained from a pure electrolyte solution on HOPG electrodes emersed from POM containing solutions after voltammetric measurements. As is in the case of GC electrodes, the cathodic peak currents of dotted lines have a linear relationship with scan rates (insets) and exhibit smaller peak separations than those of solid lines.

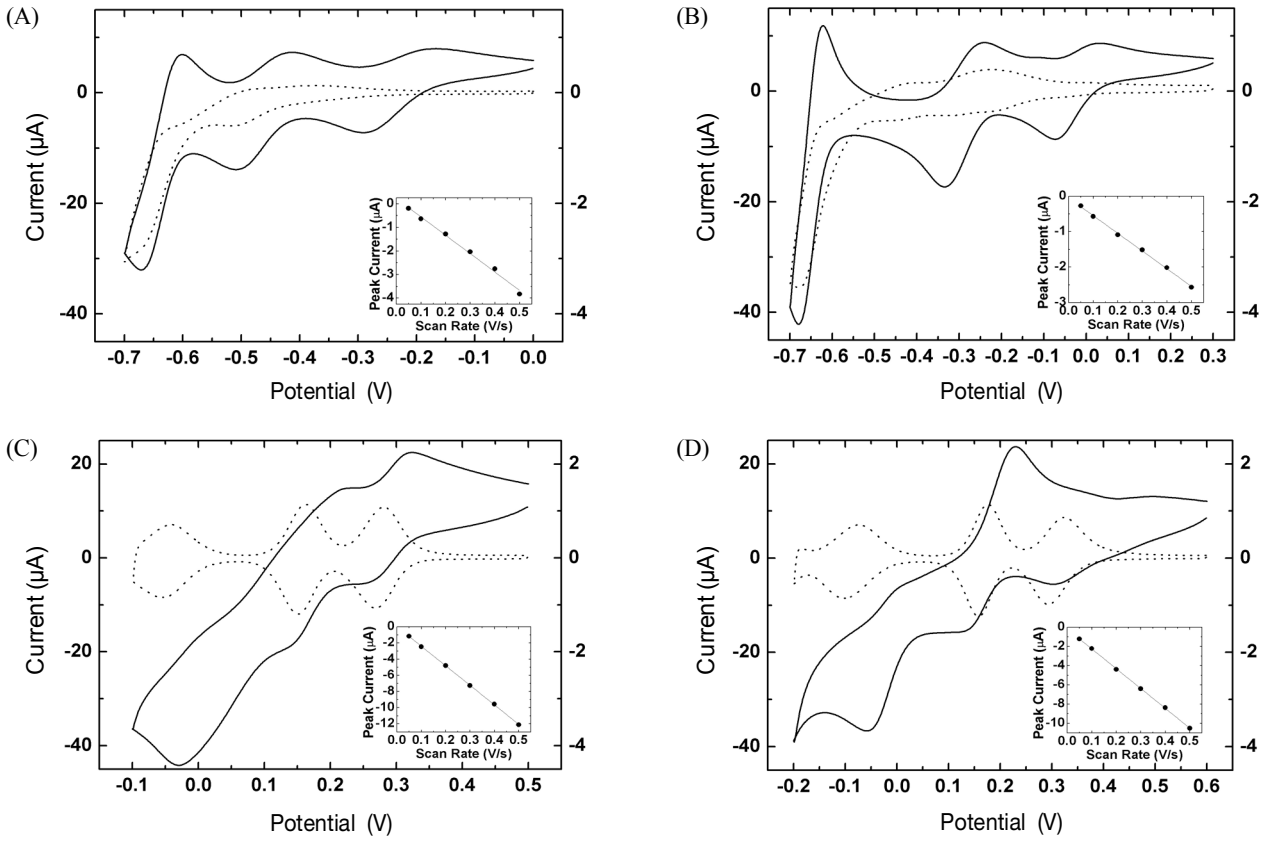

Figure 3. Cyclic voltammograms obtained from (solid line, left current axis) 1 mM POM + 0.1 M H_2SO_4 solutions on HOPG electrodes and (dotted line, right current axis) 0.1 M H_2SO_4 solutions on POM-adsorbed HOPG electrodes. (A) $SiW_{12}O_{40}^{4-}$, (B) $PW_{12}O_{40}^{3-}$, (C) $SiMo_{12}O_{40}^{4-}$, and (D) $PMo_{12}O_{40}^{3-}$. The scan rate was 0.05 V/s. The insets show the scan rate dependence of cathodic waves of POM adsorbed on HOPG electrodes.

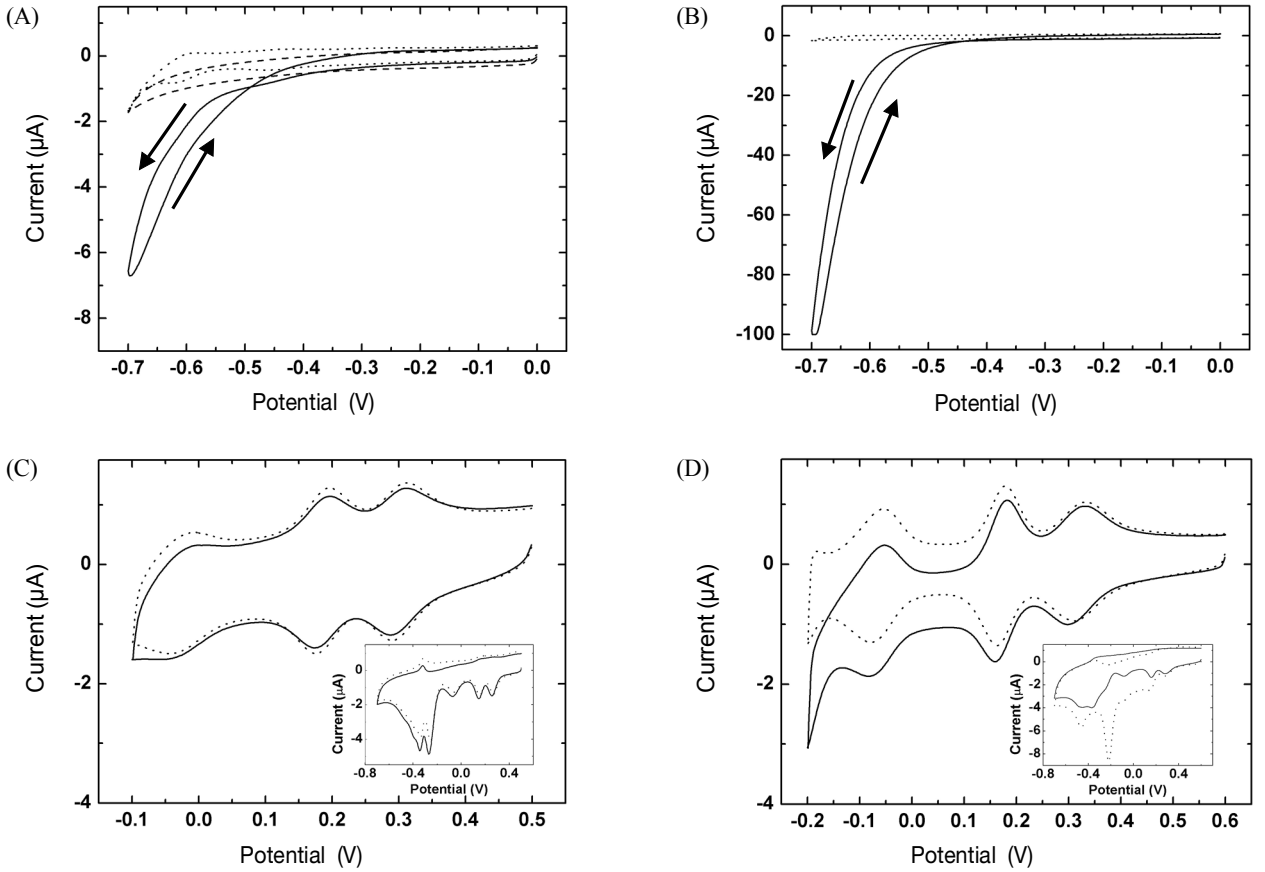

Figure 4. Cyclic voltammograms obtained from 0.1 M H_2SO_4 solutions on POM-adsorbed GC electrodes in the (dotted lines) absence and (solid lines) presence of 10 mM H_2O_2. Dashed line was obtained on a bare GC electrode in a solution containing 0.1 M H_2SO_4 and 10 mM H_2O_2. (A) $SiW_{12}O_{40}^{4-}$, (B) $PW_{12}O_{40}^{3-}$, (C) $SiMo_{12}O_{40}^{4-}$, and (D) $PMo_{12}O_{40}^{3-}$. The scan rate was 0.05 V/s.

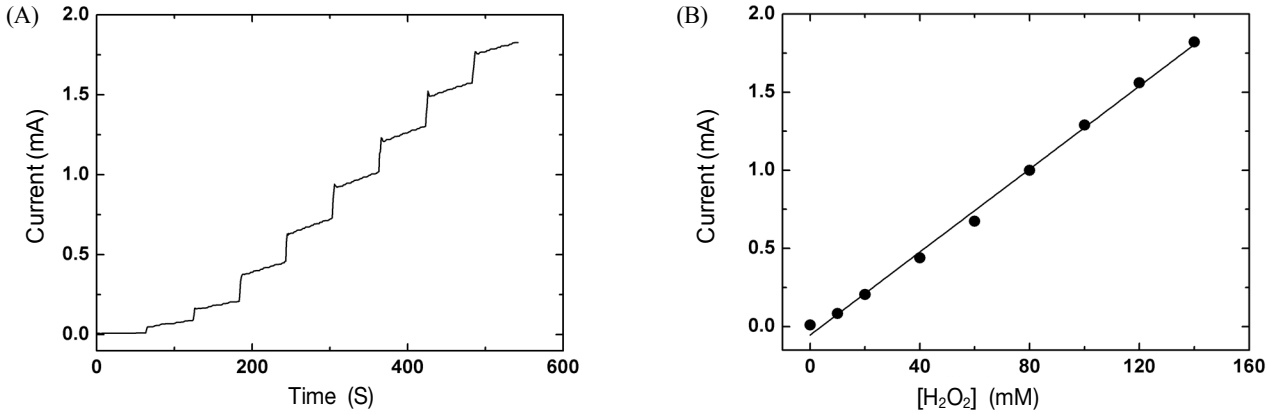

Figure 5. (A) Cathodic current obtained at 0.65 V on a $PW_{12}O_{40}^{3-}$-modified GC electrode rotated at 1000 rpm in a 0.1 M H_2SO_4 solution with successive addition of 30% H_2O_2. (B) Calibration curve obtained from experiment (A).

These indicate that the redox waves presented by dotted lines correspond to surface-confined POM species on HOPG electrodes. Midpoint potentials and peak separations for cyclic voltammograms of surface-confined POMs on HOPG electrodes are tabulated in Table 2. It is interesting that the peak separations for surface-confined $SiMo_{12}O_{40}^{4-}$ species on HOPG surfaces are *ca*. half of those found on GC surfaces, while other POMs exhibit similar peak separations on both GC and HOPG surfaces. Actually, the peak separation values of surface-confined $SiMo_{12}O_{40}^{4-}$ species on HOPG surfaces are fairly close to zero, which is expected for an ideal nernstian reaction of redox species under Lamgmuir isotherm conditions.[16] There is another unique feature in electrochemical behavior of $SiMo_{12}O_{40}^{4-}$ species on HOPG electrodes. The solution-phase cyclic voltammogram of $SiMo_{12}O_{40}^{4-}$ on HOPG surfaces is different from that obtained on GC surfaces, while other three POMs exhibit similar cyclic voltammograms both on GC and HOPG electrode surfaces. The redox current level of $SiMo_{12}O_{40}^{4-}$ species measured from solution-phase cyclic voltammograms on HOPG is quite

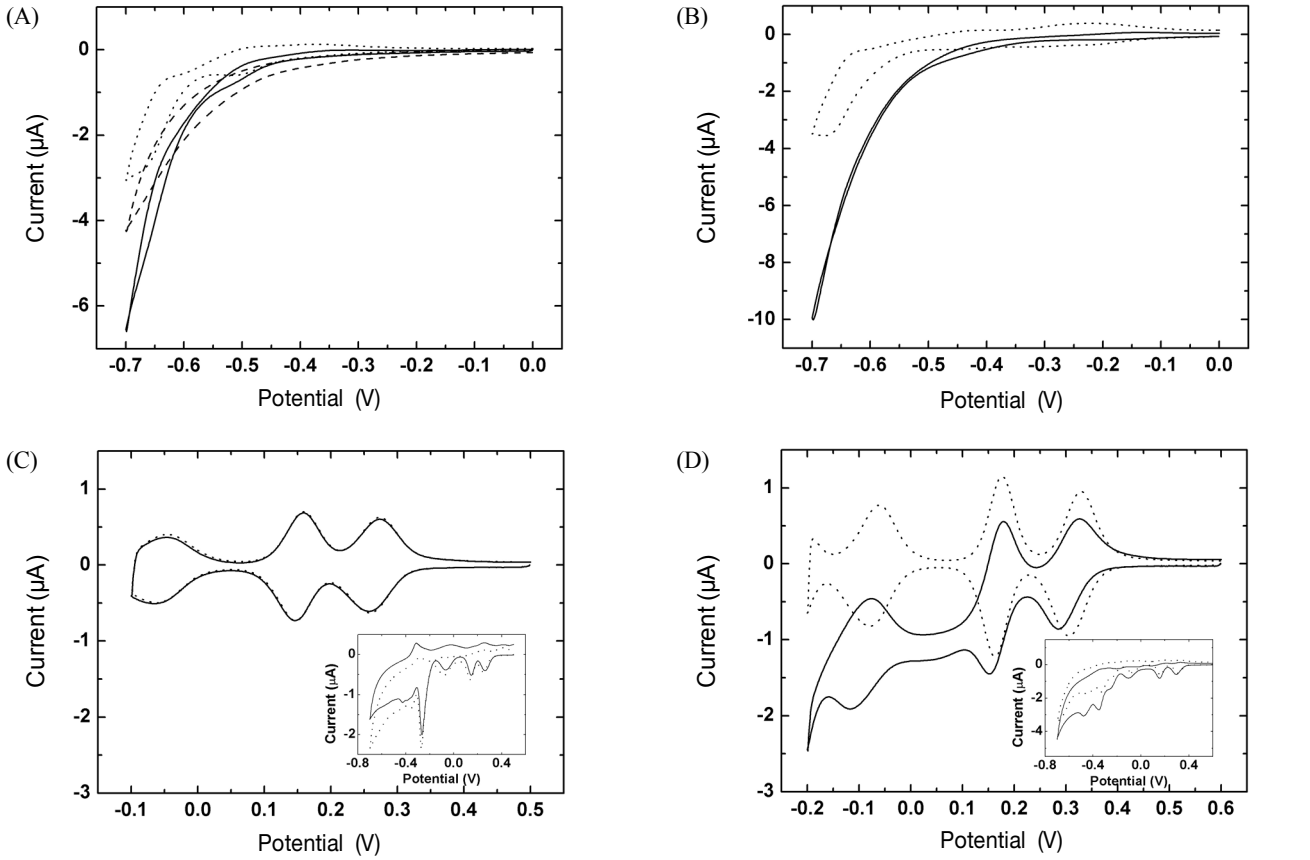

Figure 6. Cyclic voltammograms obtained from 0.1 M H_2SO_4 solutions on POM-adsorbed HOPG electrodes in the (dotted lines) absence and (solid lines) presence of 10 mM H_2O_2. Dashed line was obtained on a bare HOPG electrode in a solution containing 0.1 M H_2SO_4 and 10 mM H_2O_2. (A) $SiW_{12}O_{40}^{4-}$, (B) $PW_{12}O_{40}^{3-}$, (C) $SiMo_{12}O_{40}^{4-}$, and (D) $PMo_{12}O_{40}^{3-}$. The scan rate was 0.05 V/s.

smaller than that measured on GC surfaces. In separate experiments, we found that the electron transfer of negatively charged species, $Fe(CN)_6^{3-}$, through $SiMo_{12}O_{40}^{4-}$-modified HOPG surfaces is prohibited and the resulting redox currents decrease compared to those measured on $SiMo_{12}O_{40}^{4-}$ modified GC surfaces.[21] The decrease of redox currents on $SiMo_{12}O_{40}^{4-}$-modified HOPG surfaces was not observed for positively charged species such as $Ru(NH_3)_6^{3+}$. We tentatively ascribed the decrease of redox currents of $SiMo_{12}O_{40}^{4-}$ species in solution-phase cyclic voltammograms to the inhibition of electron transfer due to the electrostatic repulsion by negatively charged $SiMo_{12}O_{40}^{4-}$-adlayers strongly adsorbed on HOPG surface. More detailed studies on electron transfer behaviors through $SiMo_{12}O_{40}^{4-}$-modified electrode surfaces will be published elsewhere in the future.

The surface coverage of POMs on HOPG surfaces is evaluated from the charge density under the redox peaks of dotted lines in Figure 3 and tabulated in Table 2. Although there are some variations in the values of relative surface coverage, the amount of molibdate POMs adsorbed on HOPG surfaces is larger than that of tungstate POMs. Comparing the relative coverages of POMs between GC and HOPG surfaces, we noticed that HOPG surfaces exhibit higher coverages than GC surfaces in general. Considering the reduced peak separation values of surface-confined POMs on HOPG compared to GC surfaces, as well as the increase of the surface coverages, we assume that the interaction of POMs on HOPG might be stronger than on GC surfaces.

Catalytic activities of Keggin POMs adsorbed on electrode surfaces. We further investigated the electrocatalytic activity of surface-confined POM species toward electroreduction of hydrogen peroxide. As shown by dashed lines in Figure 4, the direct reduction of hydrogen peroxide is severely inhibited on bare GC electrode surfaces. The surface-confined POM species on GC surface exhibited a certain degree of electrocatalytic activity for hydrogen peroxide reduction. The solid lines in Figure 4 were obtained in a solution containing 0.1 M H_2SO_4 and 10 mM H_2O_2. For $PMo_{12}O_{40}^{3-}$ species, the electrocatalytic current was observed at potentials more negative than 0.2 V, at which the $PMo_{12}O_{40}^{3-}$ is reduced to $PMo_{12}O_{40}^{7-}$ (Figure 4D). This observation is in agreement with other experimental data previous reported for electrocatalysis of phosphomolibdate POMs toward electroreduction of hydrogen peroxide.[6,22,23] Despite the activation of the catalysis due to the adsorption of phosphomolibdate POMs, the overall rate constant of the peroxide reduction is still small. A similar electrocatalytic activity was observed on $PW_{12}O_{40}^{3-}$-modified GC surfaces, where the electrocatalytic current start to increase at around −0.4 V as shown in Figure 4B. At this potential, the $PW_{12}O_{40}^{3-}$ is reduced to $PW_{12}O_{40}^{5-}$ as described above. Both of the phospho-series POMs show catalytic activities after two reduction steps, however, the catalytic current level of $PW_{12}O_{40}^{3-}$ is higher than that of $PMo_{12}O_{40}^{3-}$ under the same amount of hydrogen peroxide. Considering

that the surface coverage of $PW_{12}O_{40}^{3-}$ is lower than that of $PMo_{12}O_{40}^{3-}$, the catalytic efficiency of the former species is quite higher than the latter. We extended the potential of $PMo_{12}O_{40}^{3-}$-modified GC electrode surface down to −0.7 V to examine the possible enhancement of electrocatalysis at negative potential regions; however, no further electrocatalytic current was observed. Upon the excursion of potential more negative than -0.2 V, several ill-defined redox waves were observed, which indicate the decomposition of $PMo_{12}O_{40}^{3-}$ species adsorbed on the electrode surface.[15]

Figure 4A and C shows the electroreduction of peroxide on GC electrode surfaces modified with silico-series POMs. Differently from $PMo_{12}O_{40}^{3-}$ species, $SiMo_{12}O_{40}^{4-}$ species do not exhibit electrocatalytic effect for peroxide reduction on GC surfaces. $SiW_{12}O_{40}^{4-}$-modified GC surfaces exhibit electrocatalysis after -0.5 V, at which the $SiW_{12}O_{40}^{4-}$ is reduced to $SiW_{12}O_{40}^{6-}$. This catalytic behavior of $SiW_{12}O_{40}^{4-}$ is similar to that observed for $PW_{12}O_{40}^{3-}$, however, the catalytic efficiency is orders of magnitude smaller than $PW_{12}O_{40}^{3-}$. Among the four Keggin POMs, the highest catalytic efficiency for peroxide was achieved for surface-confined $PW_{12}O_{40}^{3-}$ species. Figure 5A shows the cathodic current obtained on a $PW_{12}O_{40}^{3-}$-modified GC electrode rotated at 1000 rpm in a 0.1 M H_2SO_4 solution with successive addition of 30% H_2O_2. The current response is proportional to the concentration of hydrogen peroxide as shown in Figure 5B. There have been several attempts to utilize the phosphormolibdate POMs for the quantitative detection of hydrogen peroxide.[6,23] In previous cases, the sensitivity is low due to the poor catalytic efficiency and the detection limits were relatively high. $PW_{12}O_{40}^{3-}$-modified GC electrode exhibits a higher sensitivity and lower detection limit at the expense of more negative operating potentials.

Figure 6 shows the catalytic activity of surface-confined POM species on HOPG electrode surfaces. The general trend of HOPG surfaces modified with POMs for electrocatalysis of peroxide reduction is similar to that observed on GC surfaces. The cathodic current of hydrogen peroxide on a bare HOPG surface is slightly larger than that on a GC surface as shown in Figure 6A. Upon the adsorption of tungstate POMs on HOPG surfaces, catalytic activities are observed and the onset of electrocatalysis occurs at similar potentials as found on GC electrode surfaces. However, the catalytic efficiency of tungstate POMs confined on HOPG surfaces are lower compared to POMs confined on GC surfaces. Especially, $PW_{12}O_{40}^{3-}$ species adsorbed on HOPG surfaces exhibit an order of magnitude smaller catalytic activity than on GC surface. Both of tungstate POMs give similar catalytic activities for peroxide electroreduction on HOPG surfaces. $PMo_{12}O_{40}^{3-}$ species confined on HOPG surfaces is active, while $SiMo_{12}O_{40}^{4-}$ is not active for electroreduction of hydrogen peroxide. The electrocatalytic behaviors of molibdate POMs confined on HOPG surfaces are same as those observed on GC surfaces down to −0.7 V.

Conclusions

We investigated the interactions between four representative Keggin-type POMs and carbon based electrodes surfaces. Molibdate series POMs ($SiMo_{12}O_{40}^{4-}$ and $PMo_{12}O_{40}^{3-}$) strongly adsorb on GC and HOPG surfaces, while the interaction between these two surfaces and tungstate series POMs ($SiW_{12}O_{40}^{4-}$ and $PW_{12}O_{40}^{3-}$) is relatively weak. The interaction of POMs on HOPG surfaces is stronger than that on GC surfaces. The adsorption of $SiMo_{12}O_{40}^{4-}$ species on HOPG surfaces is unusually strong and the surface-confined $SiMo_{12}O_{40}^{4-}$ layers inhibit electron transfer from $SiMo_{12}O_{40}^{4-}$ species in solution phase. POM species adsorbed on surfaces shows a certain degree of electrocatalytical activities toward electroreduction of hydrogen peroxide. The $PW_{12}O_{40}^{3-}$ species adsorbed on GC electrode surfaces exhibited an order of magnitude higher catalytic activity than other systems. The present study will provide useful information on the application of Keggin POMs in chemically modified electrodes based on carbon based material such as carbon nanotubes and graphenes.

Acknowledgments. This work was supported by the Korea Research Foundation Grant funded by the Korean Government (MOEHRD, Basic Research Promotion Fund) (KRF-2007-331-C00178). This work was supported by the research grant of the Chungbuk National University in 2007.

References

1. Pope, M. T. *Heteropoly and Isopoly Oxometalates*; Springer-Verlag: Berlin, 1983.
2. Mizuno, N.; Misono, M. *Chem. Rev.* **1998**, *98*, 199.
3. Coronado, E.; Gomez-Garcia, C. J. *Chem. Rev.* **1998**, *98*, 273.
4. Keita, B.; Nadjo, L.; Belanger, D.; Wilde, C. P.; Hilaire, M. *J. Electroanal. Chem.* **1995**, *384*, 155.
5. Rong, C. Y.; Anson, F. C. *Inorg. Chim. Acta* **1996**, *242*, 11.
6. Martel, D.; Sojic, N.; Kuhn, A. *J. Chem. Educ.* **2002**, *79*, 349.
7. Ge, M. H.; Zhong, B. X.; Klemperer, W. G.; Gewirth, A. A. *J. Am. Chem. Soc.* **1996**, *118*, 5812.
8. Ge, M.; Niece, B. K.; Wall, C. G.; Klemperer, W. G.; Gewirth, A. A. *Mater. Res. Soc. Symp. Proc.* **1997**, *451*, 99.
9. Lee, L.; Gewirth, A. A. *J. Electroanal. Chem.* **2002**, *522*, 11.
10. Fattakhova-Rohlfing, D.; Kuhn, A. *Carbon* **2006**, *44*, 1942.
11. Pan, D. W.; Chen, J. H.; Tao, W. Y.; Nie, L. H.; Yao, S. Z. *Langmuir* **2006**, *22*, 5872.
12. Jianying, Q.; Xiangqin, Z.; Baifeng, L.; Shaojun, D. *Anal. Chim. Acta* **2007**, *599*, 51.
13. Ernst, A. Z.; Sun, L. S.; Wiaderek, K.; Kolary, A.; Zoladek, S.; Kulesza, P. J.; Cox, J. A. *Electroanalysis* **2007**, *19*, 2103.
14. Wlodarczyk, R.; Chojak, M.; Miecnikowski, K.; Kolary, A.; Kulesza, P. J.; Marassi, R. *J. Power Sources* **2006**, *159*, 802.
15. Sadakane, M.; Steckhan, E. *Chem. Rev.* **1998**, *98*, 219.
16. Bard, A. J.; Faulkner, L. R. *Electrochemical Methods*, 2nd ed.; John Wiley & Sons: New York, 2001.
17. Lee, L.; Wang, J. X.; Adzic, R. R.; Robinson, I. K.; Gewirth, A. A. *J. Am. Chem. Soc.* **2001**, *123*, 8838.
18. Kim, J.; Gewirth, A. A. *Langmuir* **2003**, *19*, 8934.
19. Cline, K. K.; McDermott, M. T.; McCreery, R. L. *J. Phys. Chem.* **1994**, *98*, 5314.
20. Xu, J. S.; Chen, Q. Y.; Swain, G. M. *Anal. Chem.* **1998**, *70*, 3146.
21. Choi, S.; Kim, J., unpublished result.
22. Sun, C. Q.; Zhao, J. H.; Xu, H. D.; Sun, Y. P.; Zhang, X.; Shen, J. C. *J. Electroanal. Chem.* **1997**, *435*, 63.
23. Martel, D.; Kuhn, A. *Electrochim. Acta* **2000**, *45*, 1829.